New solvothermal flow synthesis of strontium titanate nanoparticles based on the use of acetylacetonate precursors in water/ethanol mixture

Arnaud Dandre, Gilles Philippot, Mario Maglione, Jean-Marc. Bassat, Walid Baaziz, Ovidiu Ersen, Cyril Aymonier

The Journal of Supercritical Fluids 213 (2024) 106353

Contents lists available at ScienceDirect

The Journal of Supercritical Fluids

journal homepage: www.elsevier.com/locate/supflu

New solvothermal flow synthesis of strontium titanate nanoparticles based on the use of acetylacetonate precursors in water/ethanol mixture

A. Dandre [a], G. Philippot [a], M. Maglione [a], J.M. Bassat [a], W. Baaziz [b], O. Ersen [b], C. Aymonier [a,*]

[a] Univ. Bordeaux, CNRS, Bordeaux INP, ICMCB, UMR 5026, F-33600 Pessac, France
[b] IPCMS, UMR 7504 CNRS - Université de Strasbourg, F-67034 Strasbourg, France

HIGHLIGHTS

- Strontium titanate ($SrTiO_3$) is a fascinating material for "green" applications.
- A new and simple supercritical solvothermal flow synthesis using acetylacetonate precursors.
- Unique metastable nanoparticles of strontium titanate with unusual thermal stability.
- In-situ TEM investigation of metastable nanoparticles of strontium titanate evolution.

GRAPHICAL ABSTRACT

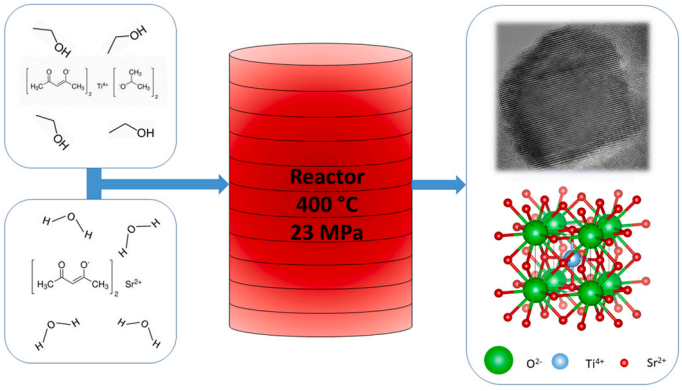

ARTICLE INFO

Keywords:
Supercritical fluid
Strontium titanate oxide
Nanocrystal
in-situ

ABSTRACT

In this study, strontium titanate ($SrTiO_3$) nanoparticles were obtained utilizing a one-step supercritical continuous solvothermal synthesis process involving acetylacetonate precursors for both strontium and titanium cations instead of the historical alkoxide ones. These precursors are expensive, difficult to access (especially for strontium isopropoxyde) and inadequately stable, forcing the use of a glove box and controlled atmospheres, which is not the case for acetylacetonates. Pure $SrTiO_3$ nanoparticles with a crystallite size of roughly 20 nm were successfully synthesized. In addition to the cubic structure of $SrTiO_3$, FTIR revealed surface functions that are typical of "wet" processes, while Raman spectroscopy showed the activation of non-centrosymmetric modes brought on by non-linear contributions. The nanoparticles show a faceted shape and are stable at elevated temperatures (up to 800 °C), according to *in-situ* high temperature XRD measurements. However, due to a chemical deficiency in strontium, titanium dioxide (TiO_2) phases are formed at higher temperatures. *In-situ* high temperature HRTEM investigations showed the existence of two populations of particles, with a better stability for the bigger-sized particles after thermal treatment as well as the sintering and restructuring of the smallest ones. Also, the microscopy results suggest the possibility of a chemical inhomogeneity within the crystallites. Overall, this study offers important new knowledge on the physicochemical characteristics of the synthesized

* Corresponding author.
E-mail address: cyril.aymonier@icmcb.cnrs.fr (C. Aymonier).

https://doi.org/10.1016/j.supflu.2024.106353
Received 4 April 2024; Received in revised form 25 June 2024; Accepted 11 July 2024
Available online 14 July 2024

$SrTiO_3$ nanoparticles and their thermal stability using a novel supercritical continuous solvothermal approach based on the use of acetylacetonate precursors.

1. Introduction

Climate change is a serious problem for our society that needs to be solved in order to reduce environmental risks [1–3]. A framework for these answers is provided by the sustainable development goals, which integrates the three pillars including environmental preservation, economic growth, and social advancement [4,5]. In this context, exploring innovative materials becomes crucial.

A fascinating material for "green" applications is the semiconductor strontium titanate ($SrTiO_3$) [6]. Strontium titanate properties are mainly defined by its perovskite structure ABO_3 corresponding to a cubic face-centered lattice where the A element corresponds to strontium and occupies the edge of the cube as the B element being the titanium in the site at the center of the cube. The oxygen is placed at the center of each face of the cube allowing the existence of octahedral corner-shared TiO_6 units making its structural specificity and backbone. It is also defined as a semiconductor due to a reasonably large band gap (reported from 3.10 eV to 3.60 eV) which can vary depending on the way it is synthetized [7]. Strontium titanate is a material of choice due to its insulating optical, thermal, electronic and dielectric properties. Due to its distinct physical and chemical characteristics, $SrTiO_3$ has attracted a lot of interest thanks to its versatility in renewable energy applications such as photocatalytic hydrogen production. It is frequently used as a component for multilayer ceramic capacitors because of its high energy density and low leakage current [8] but it can also be used in various other applications such as thermistors [9], gas sensors [10], and catalysts [11]. In optics and electronics, its physical properties are of fundamental interest [12]. It is transparent in the visible region and has a significant nonlinear optical susceptibility making it well suited for optical devices like detectors and modulators [13].

If we consider the example of electronic and ionic conductivities, these properties can be enhanced playing on the composition of the perovskite. For instance, the A site is usually substituted with rare-earth elements, which have a similar ionic radius compared to the strontium element. On the other hand, the B site substitution is achieved with transition metals which have a smaller ionic radius. This impacts the material physical properties. Its electronic properties, by the insertion of a positive hole or supplementary electron in the structure, are modified by the donor- substitute strontium titanate. It is also important to consider the possibility of tuning the electronic properties by creating vacancy sites in the lattice. For example, the cationic vacancy of the A site enhances the ionic conductivity through the creation of complementary anionic vacancies that lead to an enhanced mobility of the oxygen atoms within the lattice [14].

Diverse synthetic methods are used to produce unsubstituted and substituted $SrTiO_3$ from dry processes to "wet" ones [15–19]. Out of all the types of syntheses that exist to produce this complex material, supercritical synthesis is the most relevant technology providing nanosized crystalline particles. The supercritical continuous solvothermal synthesis allows the creation of crystallized nanoparticles of multi-cationic oxides. The first synthesis of $BaTiO_3$ (BT) using this method started in 2005 [20,21] and has been followed by deep studies of the accessible solid solutions [22] with substitution at A site, barium with strontium (BST) [23] and at B site, titanium with zirconium (BTZ) [24,25]. In both cases, the whole solid solutions of these oxides were prepared, from BT to BST and BTZ.

These syntheses were mainly achieved using alkoxide precursors such as the isopropoxides of barium and strontium. A drawback of these precursors, in addition to the environmental impact of their production, is their cost, their accessibility, their poor stability which involves a control of the work atmosphere and so the need for expensive equipment such as a glovebox in order to process them in the right way [26,27]. This new approach allows more flexibility.

The purpose of this study is to develop a new and simpler supercritical solvothermal flow synthesis method using, for the first time in the state of the art of supercritical syntheses, acetylacetonate precursors of titanium and strontium. The physicochemical properties of the produced particles with a focus on their thermal stability are discussed using numerous characterization techniques such as X-ray diffraction (XRD), Fourier-Transform Infrared (FTIR) and Raman spectroscopies, Inductively Coupled Plasma-Optical Emission Spectrometry (ICP-OES) and Transmission Electron Microscopy (TEM). Using acetylacetonate precursors gives access to material with unprecedented physicochemical properties.

2. Materials and method

2.1. Materials

Strontium (II) acetylacetonate hydrate (Sigma-Aldrich), Titanium (IV) bis(acetylacetonate) diisopropoxide in 75 wt% solution in 2-propanol for synthesis (Sigma-Aldrich), absolute ethanol (Scharlau, ≥99 wt%) and deionized water were used to synthesize the nanoparticles of $SrTiO_3$ with the supercritical continuous solvothermal technology.

2.2. Method

$SrTiO_3$ nanoparticles were synthesized using an alternative method to the one detailed elsewhere [28]. The setup includes two initial lines: the first line, where the strontium precursor is dissolved in distilled water and equipped with a preheater, and the second line, where the titanium precursor is dissolved in an absolute ethanol solution. The water line is preheated to facilitate the hydrolysis step of the sol-gel reaction. This leads to a slight decrease of the original temperature of the preheater in order to avoid any degradation of the strontium precursor. A flow reactor was specially assembled for the synthesis of $SrTiO_3$ nanoparticles based on the sol-gel reaction from acetylacetonate precursors. As shown in Fig. 1, the setup consists of two initial lines where each precursor is combined with its respective solvent. The injection lines were fed with the precursor solutions using a JASCO PU-2080 PLUS pump. To regulate the amount of water and ethanol, the precursor lines were maintained at a flow rate of 6 g/min for both injection lines. The strontium + water line includes a preheater to ensure that the solution is at the desired temperature before reaching the mixing zone. Upon reaching the mixing zone, the two flows combine and pass through a hot zone reactor made up of a coil of SS-316 stainless steel tubing (1.58 mm inner diameter) with a total length of 24 m, which was placed inside a heating clamp to control the reaction temperature (400 °C). The steady pressure of 23 MPa is maintained thanks to a TESCOM back pressure regulator (BPR). The residence time in the reactor was estimated to be around 53 s for this configuration. Subsequently, the flow reaches an ice-cooled SS-316 stainless steel tubing downstream of the reactor, which leads to a sudden decrease in temperature, allowing the reaction medium to revert to the liquid phase. This sudden quenching halts nanoparticle growth and enables the recovery of the powders. Pressure control is monitored for each injection line and after the mixing area. The temperature of the reactor is controlled with the presence of thermocouples every 6 m to ensure homogeneity throughout the reactor.

2.3. Synthesis of strontium titanate nanoparticles

$SrTiO_3$ (STO) was synthesized from strontium acetylacetonate and titanium diisopropoxide bis(acetylacetonate) precursors in a supercritical ethanol/water mixture with 0.3 mol% of ethanol (controlled with the pumps flow rate) as described in Fig. 1. The critical point of such a mixture for the supercritical solvothermal continuous synthesis are calculated using the NIST software *Refprop* which gives p_c= 13.1 MPa and T_c= 297 °C. The temperature (400°C) and pressure (23 MPa) are set higher than the critical point of the mixture. The top injection line is the water line, where the strontium precursor is solubilized, injected, and preheated at a temperature of 180°C at which the strontium precursor is still stable. The bottom injection line corresponds to the ethanol line where the titanium precursor is solubilized and injected in the system. The precursor concentrations of Sr^{2+} and Ti^{4+} were fixed at $2*10^{-4}$ M at the mixing point in order to optimize the production yield and to avoid any clogging in the reactor. The obtained solutions were then treated by centrifugation at 12,000 rotations per minute to recover the nanoparticles which were dried in an oven at 80 °C for 4 h. In order to study the impact of the concentration of strontium acetylacetonate, the molar excess was studied and was modified from 1 %, 5 %, 10 %, 15 %, and up to 20 %.

2.4. Powder characterizations

Powder X-ray diffraction (PXRD) patterns were collected at room temperature on a Malvern-PANalitycal Bragg-Brentano θ-θ geometry Empyrean diffractometer equipped with a 3×15 positions sample changer and an 1Der detector over an angular range of 2θ = 8–130°. The acquisition lasted for more than 11 h. The Cu-Kα radiation was generated at 45 KV and 40 mA (λ = 0.15418 nm). The samples were prepared on a stainless-steel sample holder with a razor blade to prevent preferential orientation. Temperature dependent PXRD patterns were collected on a PANalitycal X'pert MPD Bragg-Brentano θ-θ geometry diffractometer equipped with an Anton Paar HTK16 oven and a secondary monochromator over an angular range of 2θ = 10–80°. Each acquisition lasted for about 3 h. The Cu-K_α radiation was generated at 45 KV and 40 mA (λ = 0.15418 nm). The sample was prepared on a heating filament sample holder made of platinum and flattened with a glass slide. For all the PXRD data, the database used for the phase indexation was ICDD PDF-2 using the EVA software. All the PXRD patterns were refined using the *FullProf* software. The peak profile was fitted using the Thompson-Cox-Hastings with the pseudo-Voigt function. Among the refined parameters we focused on the lattice parameters and the crystallite sizes. The crystallite sizes were calculated using the detailed MIC file of the same software.

Raman spectra were recorded at room temperature using a HR Evolution spectrometer from HORIBA with a gas laser at λ = 633 nm. The spatial resolution is specified as a confocal microscope offering submicron lateral resolution and axial confocal performance better than 2 microns. The Raman signal data were collected and analyzed using the Labspec6 software over a domain between 150 and 800 cm^{-1}.

Fourier transform infrared (FTIR) spectroscopy was used to characterize the surface properties of nanopowders. This was achieved using a Bruker equinox 55 spectrophotometer. A small amount of strontium titanate nanoparticles was ground and mixed with KBr powder in order to perform the measurements. Then the infrared (IR) signal was collected between 400 and 4000 cm^{-1} to get a wide spectral absorption domain of the sample.

Inductively Coupled Plasma Optical Emission Spectroscopy (ICP-OES) experiments were performed with an Agilent 5800 ICP-OES instrument for chemical analysis. The working coil is operating at 1500 V RMS and about 27 MHz, leading to a plasma reaching around 10,000°C. The data were analyzed using the Expert software. The mineralization followed this protocol: 10 mg of strontium titanate nanoparticles were accurately weighted and mixed with a solution composed of 10 mL of hydrochloric acid 37 wt% (Scharlau), 3 mL of nitric acid 69.5 wt% (Scharlau) and 1 mL of hydrogen peroxide solution 30 wt% (Sharlau). The solution was then heated for 4 hours at 80 °C using Environmental Express HotBlock SC154 Digestion System. The solution was then diluted to 100 mL with ultrapure water and injected in the ICP-OES device. The quantified elements were strontium using the ray at 215.283 nm and titanium using the ray at 324.199 nm.

Transmission electron microscopy was used to observe the microstructure as well as the size and morphology of the strontium titanate particles. The devices used were a TEM-JEOL 2100 equipped with a filament LABO giving a resolution of 2.5 Å and a HRTEM-FEG JEOL 2200FS equipped with a gunfield emission giving a resolution of 1.5 Å. The TEM images were obtained and analyzed using the Digital Micrograph software. Also, the samples were dispersed in ethanol before being deposited onto a copper-carbon grids. Energy-Dispersive X-ray spectroscopy was used as a complementary characterization to analyze the elemental composition of a local area of the sample. The lines used for the quantification of strontium was located at 14.140 keV and the one for titanium at 4.508 keV to reach a clear separation and quantification of the spectra.

The *in-situ* transmission electron microscopy experiments were carried out using a JEOL JEM-2100 F microscope operated at 200 kV equipped with a spherical aberration probe corrector (Cs from CEOS), high-resolution objective lens pole piece, an UltraScan 1000 CCD array

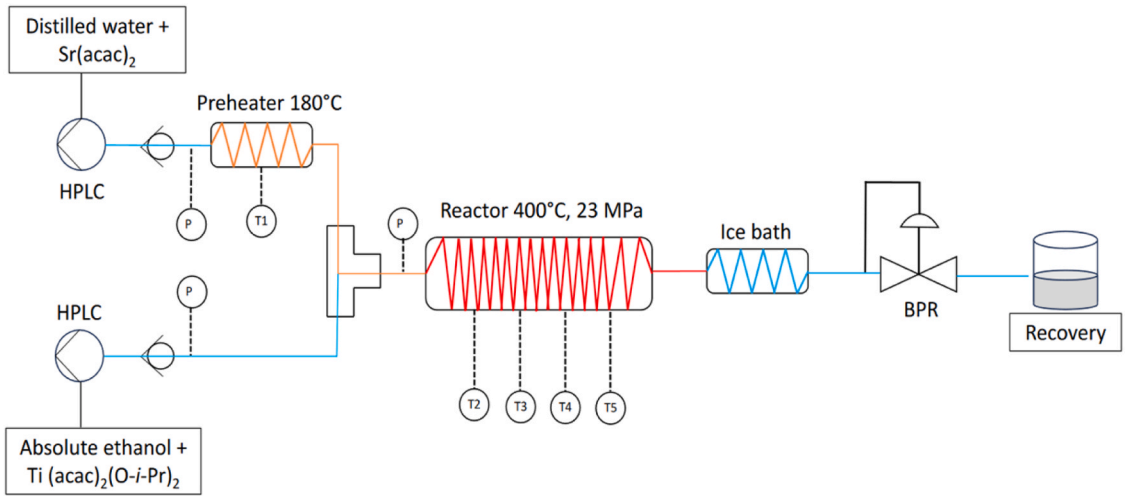

Fig. 1. Supercritical continuous solvothermal synthesis setup for the production of strontium titanate nanoparticles.

detector (GATAN) and an Centurio EDX detector (JEOL). Before the analysis, the samples were sonicated in a dichloromethane solution. For the *in-situ* observations, a Protochips Atmosphere system was used, in which the samples are suspended between two micro-electro-mechanical systems (MEMS) based closed cells made up of transparent SiNx (for observation) and SiC (for heating). The *in-situ* analysis involved several steps: firstly, the sample was heated to 100°C under vacuum, followed by the introduction of air until atmospheric pressure. In the second step, the temperature was increased to 800 °C at a rate of 10 °C per minute. Typical TEM images, on the initially chosen fragments, were recorded in the temperature range between 500 °C and 800 °C. To minimize the effects of electron beam such as contamination and sample damage, observations were made to determine the maximum electron beam dose the sample can withstand under each gaseous environment without damage. Furthermore, the *in-situ* observation areas were not continuously exposed to the electron beam, in addition, areas outside the *in-situ* observation zones were systematically observed for comparison, to check for any significant artefacts caused by electron irradiation.

3. Results and discussion

A representative PXRD pattern recorded on a $SrTiO_3$ powder synthesized using the continuous solvothermal synthesis process is shown on Fig. 2. The indexation confirms a crystallized phase of $SrTiO_3$ through the JCPS code 00–035–0734. From the Rietveld refinement, a lattice parameter of 3.911 Å, larger than the reference one of 3.905 Å for bulk, was determined [29]. This lattice expansion could be due to a size effect, well documented, for instance, in the study of Smith and al. with $BaTiO_3$ particles [30]. It is also in good agreement with the previous synthesis in supercritical conditions on $BaTiO_3$ obtained from alkoxides. Also, a crystallite size of 20 nm was calculated from the Scherrer equation. No other secondary crystallized phases are observed, which confirms the purity of the crystalline powder.

The functions located at the $SrTiO_3$ nanoparticle surface were investigated using Fourier Transform Infrared Red spectroscopy (Fig. 3). The IR signal is decomposed over different wavenumber ranges and is constituted of a main large peak located between 3750 cm^{-1} and 3000 cm^{-1} corresponding to surface hydroxyl groups and a small domain at 1600 cm^{-1} corresponding to lattice hydroxyl groups. These –OH groups are typical of "wet" processes of which the sol gel reaction is a part of. The domain between 3000 cm^{-1} and 2800 cm^{-1} corresponds to organic compounds, which could result from the precursor transformation. A narrow peak located around 1400 cm^{-1} corresponds to strontium carbonate arising from a possible side reaction of the strontium precursor inside the system. All of the above surface groups are identical to those evidenced in a previous study performed on barium titanate using isopropoxide precursors [31]. We can conclude that using this new set of precursors in an adjusted setup has no effect on the nature of the surface groups related to the "wet" processes.

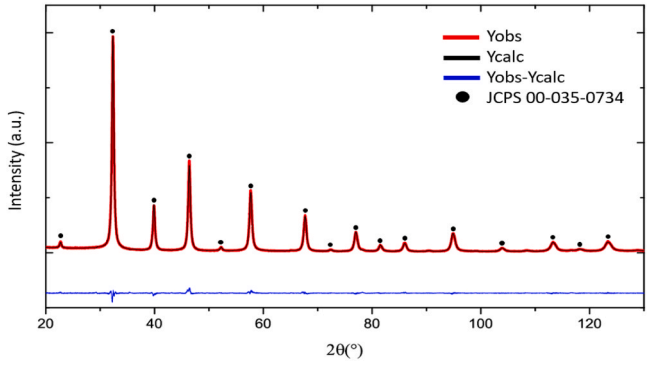

Fig. 2. Fullprof profile refinement of $SrTiO_3$ (STO) PXRD pattern in the 20° to 130° 2Θ range confirming a lattice parameter of 3.911 Å and a mean crystallite size of 20 nm.

As a complementary characterization, Raman spectra were recorded in order to study the local structure and the defect presence by indexing the longitudinal (LO) and transversal optical phonon (TO) modes in $SrTiO_3$. It is important to notice that the perovskite strontium titanate structure is cubic, so the first order Raman modes are not allowed at room temperature. However, point defects like oxygen vacancies and lattice distortion linked to the nanosize of the grains both can lead to the activation of the transversal and longitudinal modes. The modes observed in Fig. 4 are thus supposed to result from a local symmetry lowering because of lattice distortion resulting from the supercritical synthesis. Many studies have reported such an indexation on $SrTiO_3$, where the different phonon modes are attributed to different symmetries in the lattice. The first order modes are attributed to TO_2 (O-Sr-O) and TO_4 (Ti-O-Ti), whose bands are located at 171 cm^{-1} and 545 cm^{-1}, respectively. Second order modes are attributed to TO_3 (O-Sr-O) and LO_4 (Ti-O), these bands being located at 268 cm^{-1} and 794 cm^{-1}. More precisely, the TO_2 modes arise from a displacement of Sr versus the TiO_6 octahedron and the TO_4 modes are due to the bending of the octahedron following a polar axe mode. To summarize, the Raman spectra of STO shows a pure strontium titanate in which the presence of defects induces polar instability and leads to the activation of phonon modes despite the cubic structure [32–34].

The morphology and crystallinity of the synthesized strontium titanate powder were investigated using high resolution transmission electron microscopy. Fig. 5 shows three typical images: Fig. 5a reveals a large-scale view of the particles; Fig. 5b shows a focus on one crystallite; and Fig. 5c conveys a fast Fourier transform (FFT) of the image corresponding to the previous particle. The picture a) mainly shows the average morphology of the crystallites, where two populations of nanoparticles are evidenced: one includes monocrystalline particles with a faceted morphology (with an average size of 20 nm, in good agreement with the crystallite size determined from Rietveld refinement), the second population is less defined geometrically and smaller in size. The image b) is a focus on one of the faceted particles with monocrystalline characteristics while the pattern c) corresponds to its indexed fast Fourier transform which confirms the single crystalline nature of the particle. Two of the distances extracted from the FFT (3.50 Å and 2.53 Å, respectively) were used to determine the lattice parameters, *i.e.,* 2.86 Å and 3.95 Å respectively, in good agreement with the similar parameters determined by Rietveld refinement for PXRD of STO.

The thermal stability of the material was checked in order to gather more information about this novel synthesis route. To this aim, *in-situ* XRD experiments were performed from 100°C to 1200°C in air. From each XRD pattern as shown in Fig. 6, the lattice parameter and the crystallite size were determined using Rietveld refinements. The main trend stems from an expansion of the lattice parameter resulting in a shift of the peaks to smaller angle upon heating. For T > 800°C, a second crystallized phase is observed at angles between 20° and 30°. Those phases, after indexation, correspond to a TiO_2 anatase (peak located at 25.58°) and a TiO_2 rutile phase (peak at 27.59°). An increase of the anatase peak intensity is observed from 800 °C to 1100 °C followed by a decrease at 1200 °C. An increase in the intensity of the rutile peak is observed from 800 °C to 1200 °C. Another feature is the relative increase of the width of strontium titanate peaks in the same temperature range from 800°C to 1200°C showing a decrease in the crystallite size. On the inset of Fig. 6, the evolution of the crystallite size as a function of temperature from 25 °C to 1200 °C is plotted. Two distinct behaviors are observed, the first from 25 °C to 700 °C with no clear size modification, and the second from 800 °C to 1200 °C where a decrease of the crystallite size is observed from 21 to 16 nm. The starting value correlates with those deduced previously by PXRD and HRTEM, the differences being due to the accuracy and the sensitivity of each technique.

Fig. 7 shows the evolution of the lattice parameter of the strontium

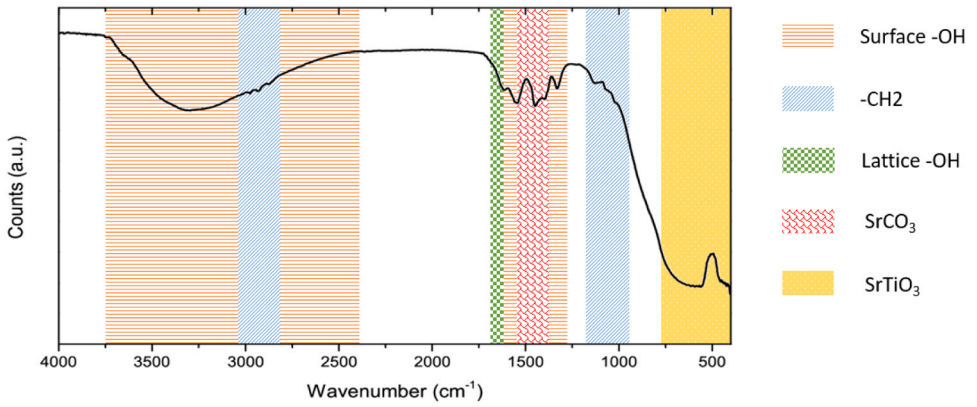

Fig. 3. IR spectrum of strontium titanate nanosized powder synthesized in the continuous supercitical solvothermal process.

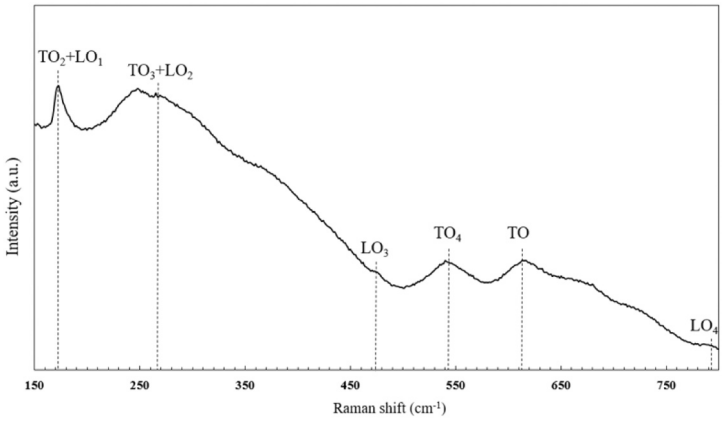

Modes	Ref [*]	Theor [**]	Exp
TO2+LO1	175	207	171
TO3+LO2	266	264	268
LO3	474	-	476
TO4	545	510	545
TO	-	635	615
LO4	795	777	794

[*] Rabuffetti et al. Chem. Mater. **2008**, *20*, 5628–5635
[**] Moreira et al. J. Phys. Chem. C **2012**, *116*, 24792–24808

Fig. 4. Indexed Raman spectrum of obtained $SrTiO_3$ nanoparticles.

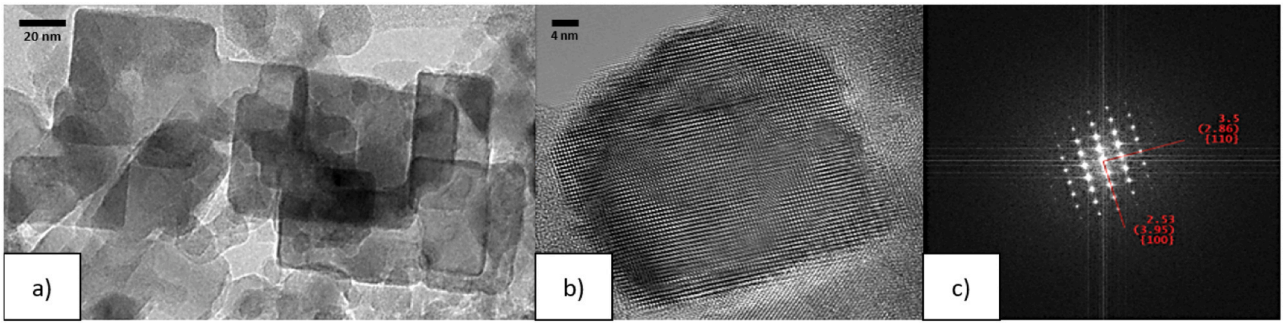

Fig. 5. Transmission electron microscopy analysis of the $SrTiO_3$ nanoparticles. a) Typical TEM image of several particles, b) High resolution image of a unique ystallite of $SrTiO_3$, c) Fast Fourrier Transform pattern of the image of the $SrTiO_3$ crystallite shown in b).

titanate phase as a function of temperature from 25 °C to 1200 °C during the heating (red square and diamond dots) and the cooling (blue triangle dots) steps. During the heating stage, a two-step behavior of the evolution of the lattice parameter is observed and correlates with the evolution of the crystallite size. From 25 °C to 700 °C, the linear lattice parameter increase is due to the thermal expansion. This is in agreement with the slope of the equation (y_1=3.19*10^{-5} K^{-1}) which is similar to the reference thermal expansion coefficient (3.23*10^{-5} K^{-1}) value of $SrTiO_3$ [35]. For T > 800°C, where a TiO_2 phase starts crystallizing, the slope decreases from 3.19*10^{-5} to 1.82*10^{-5} K^{-1} (y_2). The $SrTiO_3$ lattice is destabilized at the same time as the crystallite size decreases. This observation fully agrees with the overall diffraction peaks of the $SrTiO_3$ phase where a secondary phase TiO_2 develops. During the cooling, the atom network contracts and the lattice parameter decreases compared to the initial value observed before the crystallization of the secondary TiO_2 phase. The thermal expansion coefficient is also impacted and increases from 3.19*10^{-5} to 3.25*10^{-5} K^{-1} (y_3) which is even closer to previous quoted reference. Moreover, the initial lattice parameter (3.911 Å) decreases after the thermal treatment to 3.904 Å, a value close to the reference (3.905 Å). Those values, closer to the bulk lattice parameter as well as the thermal expansion coefficient obtained after the thermal treatment, is probably the consequence of a reorganization of the structure and a disappearance of part of the defects in the lattice.

ICP-OES measurements were performed to quantify the chemical content of strontium and titanium in the studied powders. The strontium titanate was mineralized as well as a commercial nanopowder SIGMA (<100 nm particle size) which was used as a reference. The experiments were duplicated three times per sample to have a coherent average value

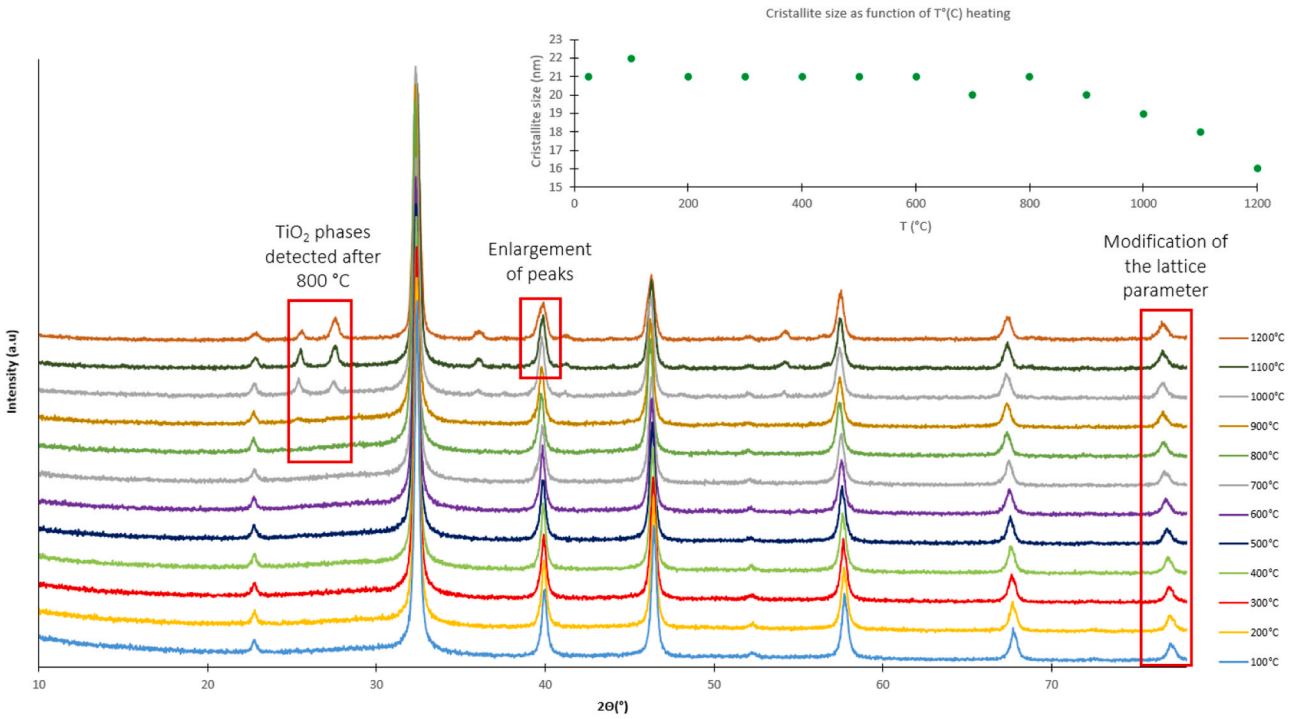

Fig. 6. In-situ high temperature X-ray diffraction of STO with the evolution of the crystallites size on upper corner as a function of temperature.

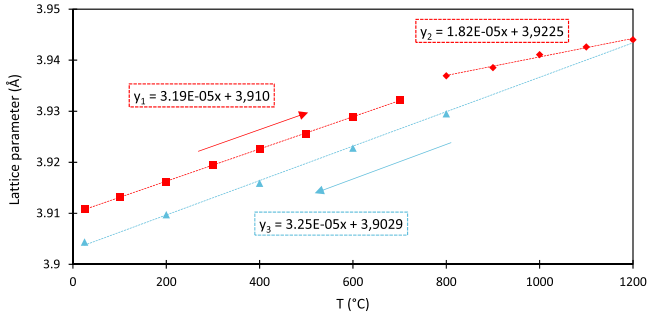

Fig. 7. Evolution of the lattice parameter of STO as a function of the temperature during the heating (red) and cooling (blue) steps.

as well as to confirm the total mineralization of the powder. The ratio Sr/Ti found for the commercial powder is close to one, as expected, confirming thus the viability of the mineralization process. The ratio found for the powder synthesized in this work is equal to 0.6, evidencing a large deficiency of strontium in the powder. This could explain the evolution of the material above 800°C (supposed to be stable at 1500 °C) where there is a crystallization of titanium dioxide. In fact, this stoichiometry could cause a "transformation" of the nanocrystalline strontium titanate due to the release of titanium, which occurs easily for T > 800 °C. This type of highly A-site deficient composition formed during the solvothermal and hydrothermal synthesis has been previously investigated for perovskite material such as $BaTiO_3$ [36] and $Ba_{1-x}Sr_xZrO_3$ [37].

To complete this quantitative analysis, energy dispersive spectroscopy measurements (EDS) were performed in scanning TEM to determine locally the relative amount of strontium and titanium (Fig. 8). For the studied area, the molar contents of strontium and titanium are of 42 and 58 mol%, respectively, confirming thus the strontium deficiency already seen in the global ICP-OES analysis, also at the nanoparticle level.

The lack of strontium can be explained by side reactions happening with the strontium precursor where strontium can react in the system by decomposition of the organic part forming strontium carbonate, which were identified by FTIR (Fig. 3). To try to optimize the Sr/Ti ratio, the concentration of the strontium precursor was increased following a molar excess of 1 %, 5 %, 10 %, 15 %, and 20 % compared to the titanium precursor. The harvested powder was then thermally treated at 850 °C to induce the transformation of the crystallites in order to determine the molar percentage of the TiO_2 and $SrTiO_3$ phases; a subsequent decrease of the titanium dioxide amount upon increasing the excess strontium precursor is expected. Fig. 9 shows the molar percentage of TiO_2 and $SrTiO_3$ of the synthesized powder after the thermal treatment. The table on the right focuses on the microstructural properties of each powder before and after the thermal treatment. In each case (various molar contents), the formation of TiO_2 is evidenced after the thermal treatment performed at 850 °C. The molar percent of TiO_2 was calculated from its weight percent of determined using the PXRD data. No clear trend connecting the amount of titanium dioxide and the excess of strontium acetylacetonate can be determined. Regarding the lattice parameter, there is no modification of the lattice parameter for all tested compositions and the crystallite size is relatively similar. The ICP-OES measurements were performed on each sample, and the average value of the Sr/Ti ratio is equal to 0.6, again meaning that the strontium titanate particles are Sr-deficient. It is difficult to establish a clear trend between the ICP-OES ratio and the amount of TiO_2 obtained after the thermal treatment of each powder. The PXRD data performed before the thermal treatment do not show the presence of an amorphous phase, the only phase existing before is indeed strontium titanate. Those results show that the molar excess of strontium does not influence the structural properties of the material. The difference in molar percentage of titanium dioxide formed after thermal treatment between the different samples could be explained by the possible inhomogeneous composition of the strontium titanate nanoparticles.

The *in-situ* analysis by TEM as a function of temperature gives an explicit interpretation of what is happening at the crystallite scale. As mentioned before, two types of nanoparticles can be observed on the TEM images. By following the same nanoparticle populations between 500 °C and 800 °C under air, the main phenomena observed are the sintering and the restructuration of the smallest population of

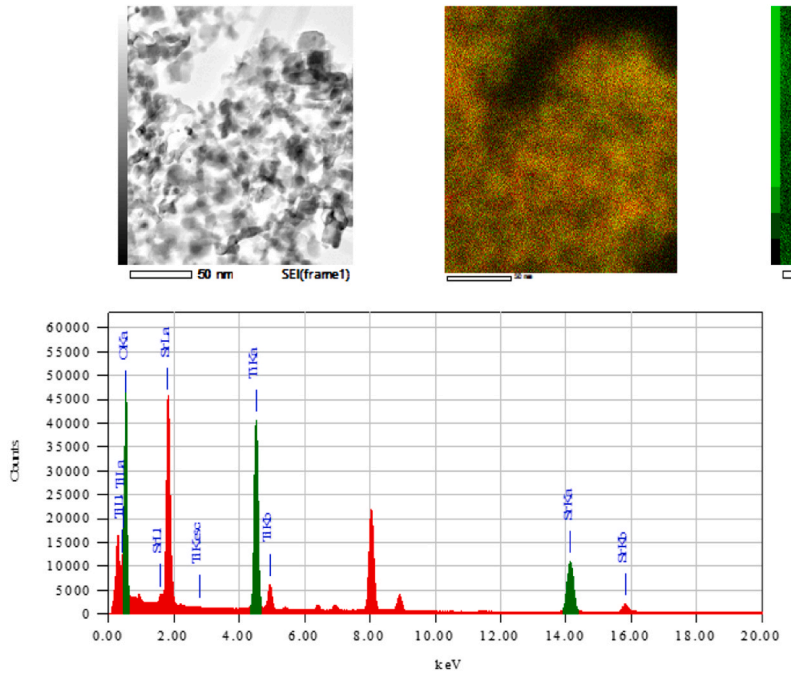

Element	(keV)	Mass%	Atom%
Ti K (ref)	4.508	43.20	58.19
Sr K	14.140	56.80	41.81
Total	-	100.00	100.00

Fig. 8. EDS spectrum (bottom left) recorded in scanning TEM mode on several STO nanoparticles (image on top left) with corresponding elemental maps (top right: Sr/Ti relative map, Sr and Ti elemental maps) and the results of the quantification analysis (bottom right).

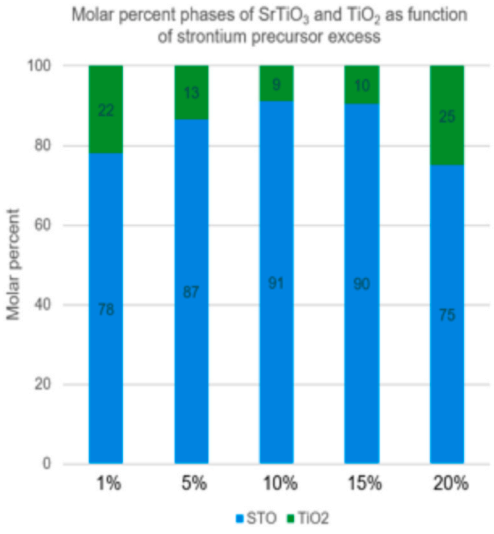

Sr excess (%at.)	1%	5%	10%	15%	20%
a (Å)	3.911	3.911	3.911	3.911	3.911
a after (Å)	3.909	3.909	3.909	3.909	3.909
Size (nm)	21	23	22	22	20
Size after (nm)	25	24	23	23	22
Sr/Ti (ICP-OES)	0.61	0.55	0.68	0.61	0.62

Fig. 9. Molar percents of the $SrTiO_3$ and TiO_2 after thermal treatment of STO nanoparticles at 850 °C (left), the results were obtained from the XRD pattern refinement and by ICP-OES (right).

nanoparticles (images c and e), in agreement with the structural evolution observed by *in-situ* PXRD at 800 °C. Another important observation is the stability of the biggest particles regarding their size and morphology from 150 °C to 800 °C. On Fig. 10, faceted particles of 20 nm are observed (images b and d). At 800 °C, the monocrystalline nature seems impacted since the shape of the particles becomes considerably less defined than before. In order to exclude a possible influence of the electron beam during the thermal treatment, an image of an area not exposed to the electron beam during the *in-situ* monitoring has been taken before and after. The aggregates show the same type of behavior, meaning the vanishing or sintering of the small particles. As no PXRD signature (nor Raman) corresponding to the presence of titanium dioxide was detected in this sample, the amorphous population could be attributed to metastable particles of strontium titanate with a lower Sr/Ti ratio. This second population may have been synthesized thanks to the fast reaction in the supercritical conditions leading to the stabilization of the particles with a lower ratio of Sr/Ti.

4. Conclusion

Using supercritical fluids in continuous flow and adapting the set-up to the use of acetylacetonate precursors allowed us to obtain unique metastable nanoparticles of strontium titanate with unusual thermal stabilities. PXRD and Raman characterizations evidenced a pure phase of strontium titanate, while FTIR confirmed surface properties characteristic of a "wet process". The HR-TEM characterizations showed the presence of two types of nanocrystallites: a first type with a faceted morphology and a second one with a less defined shape. The EDS and

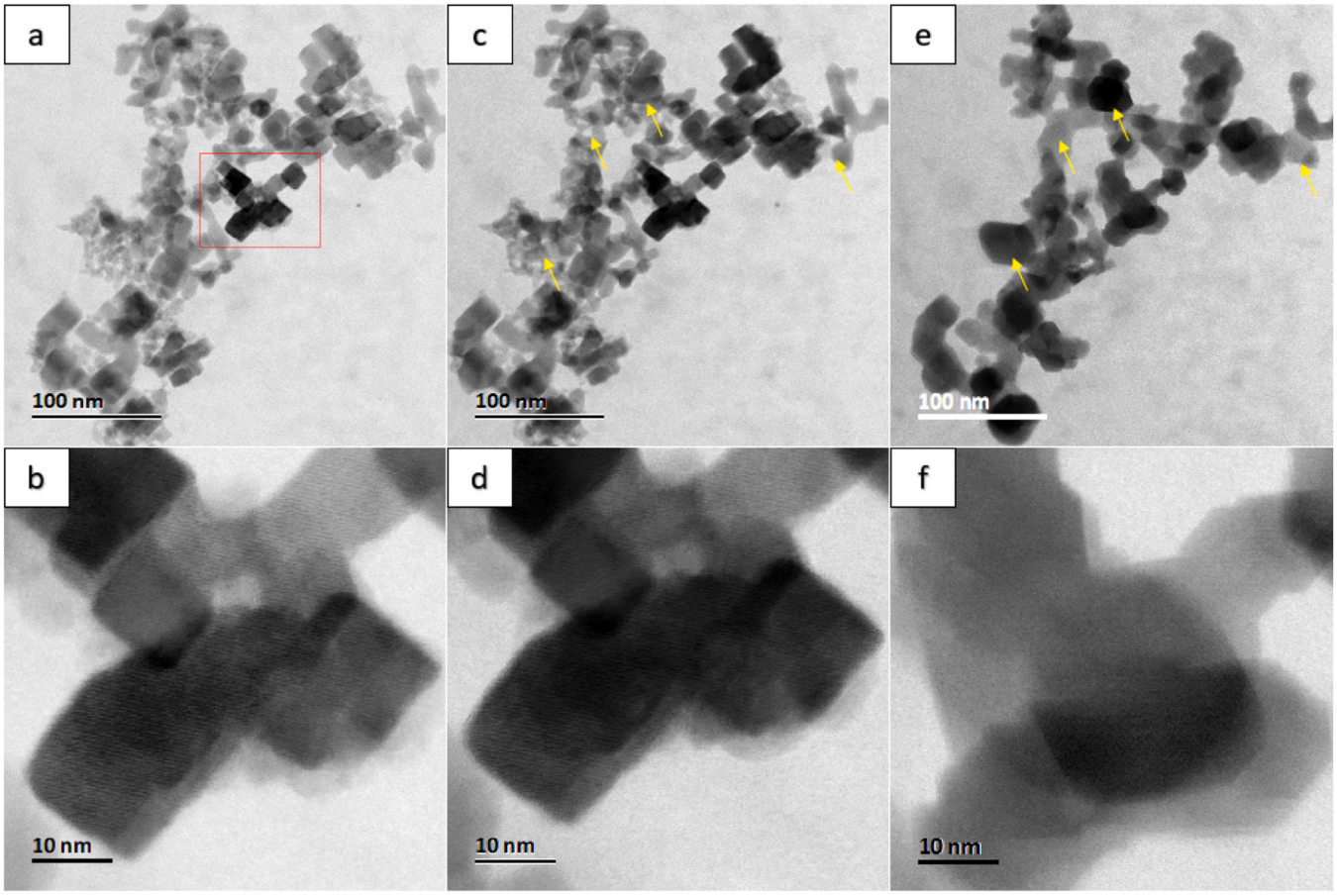

Fig. 10. In-situ high temperature TEM monitoring of an aggregate of STO nanoparticles. Images acquired at 150°C under vacuum (a and b which corresponds to the red square), at 500 °C under air (c and d) and at 800 °C under air (e and f).

ICP-OES measurements provide important information regarding the composition, highlighting a significant lack of strontium amount due to many possible scenarios, such as the synthesis of strontium carbonate inside the supercritical system. The deficiency in strontium could lead to a decreased thermal stability of the material since the formation of titanium dioxide was demonstrated at 800 °C and increased as the temperature rise. During the cooling, the amount of titanium dioxide was fixed and the lattice parameter became similar to the reference lattice value of strontium titanate after a heat treatment reaching 1200°C. This phenomenon was monitored using *in-situ* TEM with increasing temperatures and allowed us to observe a sintering of the smallest population. In the continuity of this study, a modification of the titanium precursor will be attempted in order to evaluate the impact on the reactivity of the reaction and the modification on the microstructural properties.

CRediT authorship contribution statement

Cyril Aymonier: Writing – review & editing, Validation, Supervision, Investigation, Funding acquisition, Conceptualization. **A. Dandre:** Writing – original draft, Methodology, Investigation, Formal analysis, Data curation, Conceptualization. **G. Philippot:** Writing – review & editing, Supervision, Investigation, Conceptualization. **M. Maglione:** Writing – review & editing, Validation, Supervision, Investigation, Conceptualization. **J.M. Bassat:** Writing – review & editing, Validation, Investigation, Conceptualization. **W. Baaziz:** Investigation, Conceptualization. **O. Ersen:** Writing – review & editing, Investigation, Funding acquisition, Conceptualization.

Declaration of Competing Interest

The authors declare that they have no known competing financial interests or personal relationships that could have appeared to influence the work reported in this paper.

Data availability

Data will be made available on request.

Acknowledgments

The authors acknowledge the Doctoral School of Chemistry Science of Bordeaux (EDSC), the Region Nouvelle-Aquitaine, the CNRS network “Microscopie Electronique et Sonde Atomique” (METSA, FR CNRS 3507) and the french national agency with the ANR-20-CE05-0023 grant for financial support.

References

[1] S. Rajagopalan, S.G. Al-Kindi, R.D. Brook, Air pollution and cardiovascular disease, J. Am. Coll. Cardiol. 72 (2018) 2054–2070, https://doi.org/10.1016/j.jacc.2018.07.099.

[2] J.M. Guinotte, V.J. Fabry, Ocean acidification and its potential effects on marine ecosystems, Ann. N. Y. Acad. Sci. 1134 (2008) 320–342, https://doi.org/10.1196/annals.1439.013.

[3] M. Norval, R.M. Lucas, A.P. Cullen, F.R. De Gruijl, J. Longstreth, Y. Takizawa, J. C. Van Der Leun, The human health effects of ozone depletion and interactions with climate change, Photochem. Photobiol. Sci. 10 (2011) 199–225, https://doi.org/10.1039/c0pp90044c.

[4] C. Song, Global challenges and strategies for control, conversion and utilization of CO2 for sustainable development involving energy, catalysis, adsorption and

chemical processing, Catal. Today 115 (2006) 2–32, https://doi.org/10.1016/j.cattod.2006.02.029.
[5] C. Song, Fuel processing for low-temperature and high-temperature fuel cells: challenges, and opportunities for sustainable development in the 21st century, Catal. Today 77 (2002) 17–49, https://doi.org/10.1016/S0920-5861(02)00231-6.
[6] S. Sahani, T. Roy, Y.C. Sharma, Studies on fast and green biodiesel production from an indigenous nonedible Indian feedstock using single phase strontium titanate catalyst, Energy Convers. Manag. 203 (2020) 112180, https://doi.org/10.1016/j.enconman.2019.112180.
[7] B.L. Phoon, C.W. Lai, J.C. Juan, P. Show, W. Chen, A review of synthesis and morphology of SrTiO 3 for energy and other applications, Int. J. Energy Res. 43 (2019) 5151–5174, https://doi.org/10.1002/er.4505.
[8] T.M. Correia, M. McMillen, M.K. Rokosz, P.M. Weaver, J.M. Gregg, G. Viola, M. G. Cain, A lead-free and high-energy density ceramic for energy storage applications, J. Am. Ceram. Soc. 96 (2013) 2699–2702, https://doi.org/10.1111/jace.12508.
[9] Y. Luo, X. Liu, X. Li, G. Chen, BaBiO3-doped SrTiO3-based NTC thermistors, J. Alloy. Compd. 433 (2007) 221–224, https://doi.org/10.1016/j.jallcom.2006.06.028.
[10] W. Menesklou, H.-J. Schreiner, K.H. Härdtl, E. Ivers-Tiffée, High temperature oxygen sensors based on doped SrTiO3, Sens. Actuators B Chem. 59 (1999) 184–189, https://doi.org/10.1016/S0925-4005(99)00218-X.
[11] K. Hbaieb, Exploring strontium titanate as a reforming catalyst for dodecane, Appl. Nanosci. 6 (2016) 847–854, https://doi.org/10.1007/s13204-015-0494-7.
[12] B. Zhong, C. Zuo, C. Yang, S. Yang, Y. Li, H. Yu, X. Wei, Bifunctional europium doped SrTiO3 ceramics with energy storage and photoluminescence, J. Alloy. Compd. 901 (2022) 163556, https://doi.org/10.1016/j.jallcom.2021.163556.
[13] J. Hiltunen, M. Karppinen, P. Karioja, J. Lappalainen, J. Puustinen, V. Lantto, H.L. Tuller, Electro-optical properties of BaTiO 3 -SrTiO 3 multilayer thin films for waveguide modulators, in: G.C. Righini, S.K. Honkanen, L. Pavesi, L. Vivien (Eds.), Strasbourg, France, 2008: p. 69960H. https://doi.org/10.1117/12.781163.
[14] A.V. Kovalevsky, A.A. Yaremchenko, S. Populoh, A. Weidenkaff, J.R. Frade, Effect of A-site cation deficiency on the thermoelectric performance of donor-substituted strontium titanate, J. Phys. Chem. C. 118 (2014) 4596–4606, https://doi.org/10.1021/jp409872e.
[15] K. Fröhlich, D. Machajdík, A. Rosová, I. Vávra, F. Weiss, B. Bochu, J.P. Senateur, Growth of SrTiO3 thin epitaxial films by aerosol MOCVD, Thin Solid Films 260 (1995) 187–191, https://doi.org/10.1016/0040-6090(94)06507-1.
[16] S. Ohta, T. Nomura, H. Ohta, K. Koumoto, High-temperature carrier transport and thermoelectric properties of heavily La- or Nb-doped SrTiO3 single crystals, J. Appl. Phys. 97 (2005) 034106, https://doi.org/10.1063/1.1847723.
[17] T. Moriga, S. Yabui, Y. Higashi, K.-I. Murai, Z.-W. Wang, M. Mori, A-site deficiency and structural and electrical characteristics of (Sr1-xREx)1-yTiO3 perovskites (RE=La, Nd and Sm), Int. J. Mod. Phys. Conf. Ser. 06 (2012) 85–90, https://doi.org/10.1142/S201019451200298X.
[18] K. Park, J.S. Son, S.I. Woo, K. Shin, M.-W. Oh, S.-D. Park, T. Hyeon, Colloidal synthesis and thermoelectric properties of La-doped SrTiO3 nanoparticles, J. Mater. Chem. A 2 (2014) 4217–4224, https://doi.org/10.1039/C3TA14699E.
[19] S. Singh, P. Singh, M. Viviani, S. Presto, Dy doped SrTiO3: A promising anodic material in solid oxide fuel cells, Int. J. Hydrog. Energy 43 (2018) 19242–19249, https://doi.org/10.1016/j.ijhydene.2018.08.160.
[20] H. Reverón, C. Aymonier, A. Loppinet-Serani, C. Elissalde, M. Maglione, F. Cansell, Single-step synthesis of well-crystallized and pure barium titanate nanoparticles in supercritical fluids, Nanotechnology 16 (2005) 1137, https://doi.org/10.1088/0957-4484/16/8/026.
[21] H. Reverón, C. Elissalde, C. Aymonier, C. Bousquet, M. Maglione, F. Cansell, Continuous supercritical synthesis and dielectric behaviour of the whole BST solid solution, Nanotechnology 17 (2006) 3527, https://doi.org/10.1088/0957-4484/17/14/028.
[22] G. Philippot, C. Elissalde, M. Maglione, C. Aymonier, Supercritical fluid technology: a reliable process for high quality BaTiO3 based nanomaterials, Adv. Powder Technol. 25 (2014) 1415–1429, https://doi.org/10.1016/j.apt.2014.02.016.
[23] E. Tetsi, G. Philippot, I.B. Majek, C. Aymonier, J. Audet, L. Bechou, D. Drouin, Ba1−xSrxTiO3 (x =0.4) nanoparticles dispersion for 3D integration of decoupling capacitors on glass interposer, in: 2016 6th Electron. Syst.-Integr. Technol. Conf. ESTC, IEEE, Grenoble, France, 2016: pp. 1–9. https://doi.org/10.1109/ESTC.2016.7764520.
[24] G. Philippot, M. Albino, U.-C. Chung, M. Josse, C. Elissalde, M. Maglione, C. Aymonier, Continuous BaTi1−yZryO3 (0≤y≤1) nanocrystals synthesis in supercritical fluids for nanostructured lead-free ferroelectric ceramics, Mater. Des. 86 (2015) 354–360, https://doi.org/10.1016/j.matdes.2015.07.111.
[25] G. Philippot, E.D. Boejesen, C. Elissalde, M. Maglione, C. Aymonier, B.B. Iversen, Insights into BaTi1–yZryO3 (0 ≤ y ≤ 1) synthesis under supercritical fluid conditions, Chem. Mater. 28 (2016) 3391–3400, https://doi.org/10.1021/acs.chemmater.6b00635.
[26] M. Tsang, G. Philippot, C. Aymonier, G. Sonnemann, Anticipatory life-cycle assessment of supercritical fluid synthesis of barium strontium titanate nanoparticles, Green Chem. 18 (2016) 4924–4933, https://doi.org/10.1039/C6GC00646A.
[27] M.P. Tsang, G. Philippot, C. Aymonier, G. Sonnemann, Supercritical fluid flow synthesis to support sustainable production of engineered nanomaterials: case study of titanium dioxide, ACS Sustain. Chem. Eng. 6 (2018) 5142–5151, https://doi.org/10.1021/acssuschemeng.7b04800.
[28] A. Auxéméry, G. Philippot, M.R. Suchomel, D. Testemale, C. Aymonier, Stabilization of tetragonal zirconia nanocrystallites using an original supercritical-based synthesis route, Chem. Mater. 32 (2020) 8169–8181, https://doi.org/10.1021/acs.chemmater.0c01550.
[29] Y. Wei, J. Wan, J. Wang, X. Zhang, R. Yu, N. Yang, D. Wang, Hollow multishelled structured SrTiO 3 with La/Rh Co-doping for enhanced photocatalytic water splitting under visible light, Small 17 (2021) 2005345, https://doi.org/10.1002/smll.202005345.
[30] M.B. Smith, K. Page, T. Siegrist, P.L. Redmond, E.C. Walter, R. Seshadri, L.E. Brus, M.L. Steigerwald, Crystal structure and the paraelectric-to-ferroelectric phase transition of nanoscale BaTiO3, J. Am. Chem. Soc. 130 (2008) 6955–6963, https://doi.org/10.1021/ja0758436.
[31] G. Philippot, K.M.Oe Jensen, M. Christensen, C. Elissalde, M. Maglione, B. B. Iversen, C. Aymonier, Coupling in situ synchrotron radiation with ex situ spectroscopy characterizations to study the formation of Ba1- SrTiO3 nanoparticles in supercritical fluids, J. Supercrit. Fluids 87 (2014) 111–117, https://doi.org/10.1016/j.supflu.2013.12.009.
[32] C.T. Lee, M.S. Zhang, Z. Yin, W. Zhu, Structural and vibrational properties of BaxSr1−xTiO3 nanoparticles, J. Mater. Sci. 40 (2005) 1277–1279, https://doi.org/10.1007/s10853-005-6951-z.
[33] M.L. Moreira, V.M. Longo, W.Jr Avansi, M.M. Ferrer, J. Andrés, V.R. Mastelaro, J. A. Varela, É. Longo, Quantum mechanics insight into the microwave nucleation of SrTiO3 nanospheres, J. Phys. Chem. C 116 (2012) 24792–24808, https://doi.org/10.1021/jp306638r.
[34] V. Dwij, B.K. De, S. Tyagi, G. Sharma, V. Sathe, Fano resonance and relaxor behavior in Pr doped SrTiO3: a Raman spectroscopic investigation, Phys. B Condens. Matter 620 (2021) 413265, https://doi.org/10.1016/j.physb.2021.413265.
[35] D. de Ligny, P. Richet, High-temperature heat capacity and thermal expansion of SrTiO3 and SrZrO3 perovskites, Phys. Rev. B 53 (1996) 3013–3022, https://doi.org/10.1103/PhysRevB.53.3013.
[36] A. Yoko, H. Naito, G. Seong, T. Tomai, T. Adschiri, Nucleation and coalescence of BaTiO3 using a continuous flow reactor with water–ethanol mixed solvents, J. Phys. Chem. C 125 (2021) 19489–19496, https://doi.org/10.1021/acs.jpcc.1c04914.
[37] A. Yoko, M. Akizuki, N. Umezawa, T. Ohno, Y. Oshima, Growth of Ba1−xSrxZrO3 (0 ≤ x ≤ 1) nanoparticles in supercritical water, RSC Adv. 6 (2016) 67525–67533, https://doi.org/10.1039/C6RA12288D.